

Near field and far field scattering of surface plasmon polaritons by one-dimensional surface defects

J. A. Sánchez-Gil

*Instituto de Estructura de la Materia, Consejo Superior de Investigaciones Científicas
Serrano, 121, 28006 Madrid, Spain*

A. A. Maradudin

*Department of Physics and Astronomy, and Institute for Surface and Interface Science
University of California, Irvine, CA 92697*

(April 7, 1999)

A rigorous formulation for the scattering of surface plasmon polaritons (SPP) from a one-dimensional surface defect of any shape that yields the electromagnetic field in the vacuum half-space above the vacuum-metal interface is developed by the use of an impedance boundary condition. The electric and magnetic near fields, the angular distribution of the far-field radiation into vacuum due to SPP-photon coupling, and the SPP reflection and transmission coefficients are calculated by numerically solving the k -space integral equation upon which the formulation is based. In particular, we consider Gaussian-shaped defects (either protuberances or indentations) and study the dependence of the above mentioned physical quantities on their $1/e$ half-width a and height h . SPP reflection is significant for narrow defects ($a \lesssim \lambda/5$, for either protuberances or indentations, where λ is the wavelength of the SPP); maximum reflection (*plasmon mirrors*) is achieved for $a \approx \lambda/10$. For increasing defect widths, protuberances and indentations behave differently. The former give rise to a monotonic increase of radiation at the expense of SPP transmission for increasing defect half-width. However, indentations exhibit a significant increase of radiation (decrease of SPP transmission) for half-widths of the order of or smaller than the wavelength, but tend to total SPP transmission in an oscillatory manner upon further increasing the half-width. Both the position of the maximum radiation and the oscillation period depend on the defect height, which in all other cases only affects the process quantitatively. *Light-emitters* might thus be associated with either wide indentations, or protuberances with widths that are of the order of or smaller than the wavelength.

PACS numbers: 73.20.Mf, 61.16.Ch, 78.66.Bz, 42.25.Fx

I. INTRODUCTION

In this paper, we study the scattering of surface plasmon polaritons (SPP) by surface defects. SPP are p -polarized electromagnetic (EM) waves bound to a dielectric-metal interface and caused by the surface oscillations of the electron plasma of the metal.¹ They propagate along the metal interface a distance of the order of the SPP mean free path (ranging from microns in the visible to millimeters in the infrared, of course depending also on the metal being considered), undergoing scattering processes due to surface roughness. This constitutes a classical problem of fundamental interest not only in the case of individual defects (cf. Ref. 2 and references therein), but also for periodically or randomly (or both) distributed defects.^{5,3,4,6} Furthermore, it is obviously crucial in any light scattering problem involving rough metal surfaces where roughness-induced excitation of SPP occurs. This has been explicitly shown in connection with either single defects^{7,8,9} or random corrugation,^{10,11,12,13} the latter configuration being relevant to the phenomenon of (SPP mediated) enhanced backscattering of light. In addition to that, light-SPP coupling plays a central role in other phenomena such as

anomalous transmission through metal slabs with hole arrays,^{14,15} surface-enhanced Raman scattering,^{16,17,18} or biosensing.¹⁹

In recent years, the advent of near-field optical microscopy²⁰ has opened up the possibility to study experimentally SPP in a direct manner. Among the various configurations developed, photon scanning tunneling microscopy²¹ (PSTM), basically exploiting SPP excitation in the attenuated total reflection arrangement, has made it possible to probe the SPP structure,^{22,23} localized SPP on randomly rough surfaces,²⁴ and SPP resonances in fractal colloid clusters²⁵ and single particles.^{26,27} Moreover, PSTM images have been obtained by surface-enhanced Raman scattering probing single molecules adsorbed on single nanoparticles.²⁶ PSTM in combination with direct-write lithography has made it possible to create sub-micron defects on metal surfaces.²⁸

Particularly relevant to the present work are the recent experimental studies on SPP scattering by surface defects.^{29,30,31} These studies have shown evidence of drastically distinct scattering properties depending on the defect size. Specifically, surface defects favoring SPP reflection and light coupling, called SPP mirrors

and flashlights,²⁹ respectively, have been described, as well as SPP microlenses and microcavities;³⁰ SPP Bloch waves have also been imaged in periodic arrays of surface defects.³¹ Interestingly, the possibilities of artificially creating micro-optical components for SPP have also been noted in these studies. Much has to be done, however, from the theoretical standpoint. Quite recently, calculations for circularly symmetric defects have successfully accounted for the peculiar azimuthal dependence of the radiated pattern,³² in addition, such calculations have been used to retrieve the surface profile.³³ In the case of one-dimensional surface defects, preliminary calculations have focused on the optimization of the defect size to obtain SPP mirrors and so-called light-emitters.³⁴ In this regard, it is our purpose to address in detail the SPP scattering by one-dimensional surface defects, including near-field and far-field calculations (along with energy balance) and their dependence on defect size parameters. Thus we expect not only to shed light on the experimental works mentioned above, but also to find and predict related effects.

The physical system we consider here is a planar one-dimensional metal surface with a one-dimensional defect. The surface corrugation is modeled by using a local impedance boundary condition (IBC) on a flat surface. The connection between surface impedance and real surface corrugation has been recently demonstrated,³⁵ and its validity to give accurate quantitative results has been shown in numerical calculations of grating-induced SPP-photon coupling.³ A scattering-theoretic formulation of the interaction of an SPP with the surface roughness is developed by imposing the IBC on the amplitude of the magnetic field in the vacuum region in the form of a Rayleigh expansion. Upon solving the resulting integral equation for the scattering amplitude, the magnetic field at any point in the vacuum half-space can be calculated. We will focus on the far field angular distribution and the surface field amplitudes to determine, respectively, the total radiated energy S , and the SPP reflection R_{SP} and transmission T_{SP} coefficients. By numerical simulation calculations, these quantities are computed.

The paper is organized as follows. The theoretical formulation is derived in Sec. II, and some details pertaining to the numerical procedure are given in the Appendix. In Sec. III, we show the results obtained for a single Gaussian defect and the influence of defect width and height. Finally, Section IV summarizes the conclusions drawn from this research.

II. THEORY

A. Scattering Equations

We study the scattering of a p-polarized SPP of frequency ω propagating along a flat vacuum-metal interface ($x_3 = 0$) by a one-dimensional obstacle (constant

along the x_2 -axis, see Fig. 1). Under these circumstances, the three-dimensional electromagnetic problem can be cast into a two-dimensional scalar problem in such a way that the single, nonzero component of the magnetic field amplitude $H_2(x_1, x_3)$ is the solution of the corresponding two-dimensional Helmholtz equation in the upper (vacuum) and lower (metal) half spaces. The magnetic field in vacuum is assumed to be the sum of an incoming SPP and a scattered field as follows

$$H_2^>(x_1, x_3) = \exp[ik(\omega)x_1 - \beta_o(\omega)x_3] + \int_{-\infty}^{\infty} \frac{dq}{2\pi} R(q, \omega) \exp[iqx_1 + i\alpha_o(q, \omega)x_3], \quad (1)$$

where

$$k(\omega) \equiv k^R(\omega) + ik^I(\omega) = \frac{\omega}{c} \left(1 - \frac{1}{\epsilon(\omega)}\right)^{1/2}, \quad (2)$$

$$\beta_o(\omega) = \left(k(\omega)^2 - \frac{\omega^2}{c^2}\right)^{1/2} = \frac{\omega}{c} [-\epsilon(\omega)]^{-1/2}, \quad (3)$$

and

$$\alpha_o(q, \omega) = \left(\frac{\omega^2}{c^2} - q^2\right)^{1/2} \quad |q| \leq \frac{\omega}{c} \quad (4a)$$

$$= i \left(q^2 - \frac{\omega^2}{c^2}\right)^{1/2} \quad |q| > \frac{\omega}{c}. \quad (4b)$$

Note that the expressions for the SPP wavevector components $k(\omega)$ and $\beta_o(\omega)$ in vacuum apply in the limit $|\epsilon(\omega)| \gg 1$. This stems from the fact that the continuity conditions across the interface are mapped onto a local IBC on the planar surface $x_3 = 0$ in the form

$$\left. \frac{\partial}{\partial x_3} H_2^>(x_1, x_3) \right|_{x_3=0} = -\frac{\omega}{c} \frac{1 + s(x_1)}{[-\epsilon(\omega)]^{1/2}} H_2^>(x_1, x_3)|_{x_3=0}, \quad (5)$$

where the superscript $>$ indicates the vacuum region, $-(\omega/c)[- \epsilon(\omega)]^{-1/2}s(x_1)$ is the contribution to the surface impedance associated with the obstacle, and $\epsilon(\omega)$ is the isotropic, frequency-dependent dielectric function of the metal. The IBC has been widely used in the past to model the vacuum-metal interface qualitatively, especially in the infrared region of the optical spectrum. Furthermore, it has been recently proven to be quantitatively accurate in calculations of grating-induced photon-SPP coupling³ by using the connection between surface impedance and real corrugation demonstrated in Ref. 35.

In order to calculate the scattering amplitude $R(q, \omega)$, we substitute Eq. (1) into Eq. (5), and obtain the integral equation $R(q, \omega)$ satisfies,

$$R(q, \omega) = G_0(q, \omega)V(q|k(\omega)) + G_0(q, \omega) \int_{-\infty}^{\infty} \frac{dp}{2\pi} V(q|p)R(p, \omega), \quad (6)$$

where

$$G_0(q, \omega) \equiv \frac{i\epsilon(\omega)}{\epsilon(\omega)\alpha_0(q, \omega) + i(\omega/c)[- \epsilon(\omega)]^{1/2}} \quad (7)$$

is the Green's function of the SPP on the unperturbed surface [$s(x_1) = 0$]. We have also introduced the scattering potential

$$V(q|p) \equiv \beta_0(\omega)\hat{s}(q-p), \quad (8)$$

with

$$\hat{s}(Q) = \int_{-\infty}^{\infty} dx_1 e^{-iQx_1} s(x_1), \quad (9)$$

to simplify the notation. Equation (6) can be rewritten in a more convenient manner by substituting

$$R(q, \omega) = G_0(q, \omega)T(q, \omega), \quad (10)$$

into it, so that

$$T(q, \omega) = V(q|k(\omega)) + \int_{-\infty}^{\infty} \frac{dp}{2\pi} V(q|p)G_0(p, \omega)T(p, \omega). \quad (11)$$

Equation (11), along with Eqs. (1) and (10), is the basis of our theoretical formulation.

In solving Eq. (11), it is very important how we deal with the poles appearing in the Green's function (7). First, we rewrite the latter in the form

$$G_0(q, \omega) = C(q, \omega) \left(\frac{1}{q - k(\omega)} - \frac{1}{q + k(\omega)} \right), \quad (12)$$

with

$$C(q, \omega) \equiv \frac{\epsilon(\omega)\alpha_0(q, \omega) - i(\omega/c)[- \epsilon(\omega)]^{1/2}}{2i\epsilon(\omega)k(\omega)}. \quad (13)$$

We now assume that the metal dielectric function is given by Drude's expression

$$\epsilon(\omega) = 1 - \frac{\omega_p^2}{\omega^2}, \quad (14)$$

where ω_p is the plasma frequency, in the absence of absorption losses. Therefore, in light of Eq. (2), we have to take the limit $k^I(\omega) \rightarrow 0$ in Eq. (7), to obtain

$$G_0(q, \omega) = C(q, \omega) \left(\frac{1}{q - k^R(\omega)} \Big|_P - \frac{1}{q + k^R(\omega)} \Big|_P + \pi i [\delta(q - k^R(\omega)) + \delta(q + k^R(\omega))] \right). \quad (15)$$

The first two terms on the right-hand side of Eq. (15) have meanings in the Cauchy's principal value sense, whereas the last two terms are delta functions. Once Eq. (11) is solved for $T(q, \omega)$ [we will see below how to do so numerically with the help of Eq. (15)], we proceed to calculate the electric and magnetic near fields, the SPP-photon coupling, and the SPP reflection and transmission coefficients in the following manner.

B. Near Field

The magnetic field at any point in the vacuum half-space can be straightforwardly calculated from Eq. (1), upon recalling Eq. (10), which relates $T(q, \omega)$ with the scattering amplitude $R(q, \omega)$. Then the electric field components in vacuum are easily written also as functions of $R(q, \omega)$ by means of a Maxwell curl equation as follows:

$$E_1^>(x_1, x_3) = \frac{c}{\omega} i\beta_0(\omega) \exp[ik(\omega)x_1 - \beta_0(\omega)x_3] + \frac{c}{\omega} \int_{-\infty}^{\infty} \frac{dq}{2\pi} \alpha_0(q, \omega) R(q, \omega) \times \exp[iqx_1 + i\alpha_0(q, \omega)x_3] \quad (16a)$$

$$E_2^>(x_1, x_3) = 0 \quad (16b)$$

$$E_3^>(x_1, x_3) = -\frac{c}{\omega} k(\omega) \exp[ik(\omega)x_1 - \beta_0(\omega)x_3] - \frac{c}{\omega} \int_{-\infty}^{\infty} \frac{dq}{2\pi} qR(q, \omega) \times \exp[iqx_1 + i\alpha_0(q, \omega)x_3]. \quad (16c)$$

The time-averaged Poynting vector thus reads:

$$\langle \mathbf{S} \rangle = \frac{c}{8\pi} \Re(\mathbf{E} \times \mathbf{H}^*) = \frac{c}{8\pi} \Re(-E_3 H_2^*, 0, E_1 H_2^*), \quad (17)$$

where \Re denotes the real part and the asterisk the complex conjugate.

C. Radiated energy

The total power carried away from the surface in the form of volume electromagnetic waves propagating in the vacuum region above it, per unit length of the system along the x_2 -axis is

$$P_{sc} = \int_{-\infty}^{\infty} dx_1 \langle S_3^{(sc)} \rangle = \frac{c^2}{8\pi\omega} \int_{-\omega/c}^{\omega/c} \frac{dq}{2\pi} \alpha_0(q, \omega) |R(q, \omega)|^2. \quad (18)$$

Note that only the scattered field contribution to the x_3 -component of the time-averaged Poynting vector is used. Equation (18) must be normalized by the power carried by the incident SPP per unit length along the x_2 -axis

$$P_{inc} = \int_0^{\infty} dx_3 \langle S_1^{(inc)} \rangle = \frac{c^2 k(\omega)}{16\pi\omega\beta_0(\omega)}, \quad (19)$$

where $\langle S_1^{(inc)} \rangle$ is the x_1 -component of the time-averaged Poynting vector of the incident SPP. Then the total, normalized scattered power S is given by

$$S = \frac{P_{sc}}{P_{inc}} = \int_{-\pi/2}^{\pi/2} d\theta_s \frac{\partial R}{\partial \theta_s}, \quad (20)$$

where

$$\frac{\partial R}{\partial \theta_s} = \frac{1}{2\pi} \frac{\beta_0(\omega)}{2k(\omega)} \alpha_0^2 \left(q = \frac{\omega}{c} \sin \theta_s \right) \times \left| R \left(q = \frac{\omega}{c} \sin \theta_s \right) \right|^2, \quad (21)$$

is the differential reflection coefficient (DRC), namely, the fraction of the energy of the incident SPP that is scattered into an angular region of width $d\theta_s$ about the scattering direction θ_s where the scattering angle θ_s is measured clockwise with respect to the x_3 -axis (see Fig. 1).

D. Reflection and transmission coefficients

In order to evaluate the amplitude of the reflected and transmitted SPP, we study the behavior of $H_2^>(x_1, x_3)$, Eq. (1), with the help of Eqs. (10) and (15), on the surface $x_3 = 0$. At this point, great care has to be taken when calculating the contribution to the scattered field in Eq. (2) from the Cauchy principal value integrals arising from the first two terms on the right-hand side of Eq. (15). We assume that the obstacle has a finite extent and is centered about $x_1 = 0$. If we focus on the regions $x_1 \ll 0$ and $x_1 \gg 0$ far from the obstacle, it can be shown, by working out the contributions from those integrals in the complex q -space with the help of Cauchy's theorem,³⁶ that the magnetic field is given by:

$$H_2^>(x_1, x_3 = 0) = \exp[ik^R(\omega)x_1] + r(\omega) \exp[-ik^R(\omega)x_1], \quad x_1 \ll 0 \quad (22a)$$

$$= t(\omega) \exp[ik^R(\omega)x_1], \quad x_1 \gg 0, \quad (22b)$$

where the amplitudes of the reflected and transmitted SPP, $r(\omega)$ and $t(\omega)$, respectively, are

$$r(\omega) = iT(-k^R(\omega), \omega) C(-k^R(\omega), \omega) \quad (23a)$$

$$t(\omega) = 1 + iT(k^R(\omega), \omega) C(k^R(\omega), \omega). \quad (23b)$$

Equations (22) manifest the fact that, away from the obstacle, only the incident and reflected SPP (on the left-hand side, see Fig. 1) and the transmitted SPP (on the right-hand side) propagate along the interface. The corresponding reflection and transmission coefficients are

$$R(\omega) = |r(\omega)|^2 \quad (24a)$$

$$T(\omega) = |t(\omega)|^2. \quad (24b)$$

E. Numerical Calculations

The integral equation (11) is numerically solved by converting it into a matrix equation through a quadrature scheme. The details are given in the Appendix. It should be pointed out that the discretization q -mesh is chosen in such a way that $q = \pm k^R(\omega)$ are always

points on the mesh, as required by Eq. (23). In addition, the discretization is not regular: the density of q -points around the poles at $q = \pm k^R(\omega)$ is considerably larger ($\Delta q \approx 10^{-4}\omega/c$) than it is either in the radiative region $|q| \leq \omega/c$ or in the non-radiative region away from the poles ($\Delta q \approx 10^{-2}\omega/c$). The number N of q -points needed in the numerical procedure depends not only on the accuracy required to sample the pole regions, but also on the explicit form of the obstacle, which enters in the calculation through its Fourier-transform in Eq. (9). Throughout this work, typically $N = 2600$, except for the larger defects for which up to $N = 4000$ points are employed. The convergence of the numerical results with increasing N has been checked in the most unfavorable cases.

III. RESULTS AND DISCUSSION

Note that up to now no restrictions have been imposed on the shape of the obstacle apart from its having a finite extent along the x_1 -axis. Its surface impedance function $s(x_1)$ is connected to the actual surface profile defined by $x_3 = f(x_1)$ through³⁵

$$s(x) = -\frac{1 - \epsilon(\omega)}{d(\omega)\epsilon(\omega)} [1 - d^2(\omega)D^2]^{1/2} f(x_1) + O(f^2), \quad (25)$$

where $d(\omega) = (c/\omega)[- \epsilon(\omega)]^{-1/2}$ is the optical skin depth, and $D \equiv d/dx_1$. In the case of small skin depths and surface slopes $(dD)^2 \ll 1$, the square root term on the rhs of Eq. (25) can be expanded as

$$[1 - (dD)^2]^{1/2} = 1 - \frac{1}{2}(dD)^2 - \dots - \frac{1.1.3 \dots (2n-3)}{2.4.6 \dots 2n} (dD)^{2n} + O((dD)^{2n+2}). \quad (26)$$

Then the Fourier transform of the surface impedance function, which is needed in the calculation [cf. Eq. (8)], is related to the Fourier transform $\hat{f}(Q)$ of the surface profile function through

$$\hat{s}(Q) = -\frac{1 - \epsilon(\omega)}{d(\omega)\epsilon(\omega)} \left(1 - \frac{1}{2}[-id(\omega)Q]^2 - \frac{1}{8}[-id(\omega)Q]^4 + O([-id(\omega)Q]^6) \right) \hat{f}(Q). \quad (27)$$

In what follows, we will restrict the analysis to a Gaussian defect of $1/e$ half-width a and height h :

$$f(x_1) = h \exp(-x_1^2/a^2). \quad (28)$$

In addition, unless otherwise stated, we retain in Eq. (26), and thus in Eq. (27), only the zeroth order term in the expansion in powers of $[-id(\omega)Q]^2$, as implicitly done in Ref. 34. Therefore the function $\hat{s}(Q)$ we will use in our calculations is

$$\hat{s}(Q) = \pi^{1/2} s_0 a \exp[-(aQ)^2/4], \quad (29a)$$

with

$$s_0 = -\frac{1 - \epsilon(\omega)}{\epsilon(\omega)} \frac{h}{d(\omega)}. \quad (29b)$$

It should be emphasized that the approximation involved in retaining only the lowest order term in the expansion (26) affects only the expression connecting the surface impedance with the real surface profile, the scattering formulation being rigorous and energy conserving (recall that losses are not accounted for) whatever the surface impedance is. Nonetheless, inasmuch as we wish to be able to quantitatively relate our results with real defect sizes, the effect of neglecting the higher order terms in Eq. (26) has to be determined. We have thus verified in the most unfavorable cases that including the first order term in $[-id(\omega)Q]^2$ in Eq. (27) barely modifies our calculations.

In order to establish the accuracy and efficiency of the numerical calculations based on the formulation above, we first calculate the function $T(q, \omega)$ [cf. Eq. (11)], following the numerical procedure outlined in Sec. II and the Appendix, for two Gaussian defects of half-width $a/\lambda = 0.1$ and heights $h/\lambda = \pm 0.05$ (protuberance and indentation of equal height/depth), where λ is the wavelength of the SPP. From these results, the SPP reflection and transmission coefficients are straightforwardly calculated [cf. Eqs. (23) and (24)], along with the DRC [cf. Eqs. (10) and (21)]. Furthermore, the magnetic and electric fields at any point in the vacuum half-space can be calculated from Eqs. (1) and (16) by using Eq. (10). In Fig. 2 we present the results thus obtained for the magnetic field intensities at the vacuum-metal interface in the vicinity of the Gaussian defects, and for the angular distribution of the scattered field in the far field. From the surface magnetic field in Fig. 2(a), it is evident that both surface defects reflect back part of the incoming SPP, which interferes with the incoming SPP giving rise to the oscillatory pattern to the left of the defect (negative x_1 -axis). Near the defect the magnetic field is perturbed. The outgoing transmitted SPP is seen to the right of the defect. The SPP reflection and transmission coefficients are: $R_{SP} = 0.0025$ and $T_{SP} = 0.9825$ for the protuberance, and $R_{SP} = 0.0041$ and $T_{SP} = 0.9728$ for the indentation. In Fig. 2(b) a fairly uniform angular distribution of the DRC is observed (this will be discussed below). The total scattered power calculated from Eq. (20) is $S = 0.0149$ for the protuberance, and $S = 0.0231$ for the indentation. Energy conservation is thus satisfied within a 0.01% error.

We find that away from the vicinity of the defect, the magnetic field is fully described by either the interference between incoming and reflected SPP on the left-hand side, or by merely the transmitted SPP on the right-hand side. This corroborates, as expected, our argument in Sec. IID leading to Eqs. (22). The reflection and

transmission coefficients are thus calculated from Eqs. (23) and (24).

A. Energy balance dependence on defect size

The question now arises naturally as to how efficient the surface defect is in coupling the incoming SPP into the different outgoing channels (either SPP or photons), or conversely, what the appropriate defect parameters are that maximize or minimize those channels; this is crucial for both an understanding of the scattering process and the design of practical devices. To that end, we have studied the dependence of the scattering coefficients R_{SP} , T_{SP} , and S on the defect half-width a for both Gaussian protuberances and indentations of different heights $h/\lambda = 0.05$ and 0.2 . The results are shown in Fig. 3. Several general features are evident from these results.

First, SPP reflection is relevant only for very narrow defects, $a < \lambda/5$, for either protuberances or indentations. Indeed there is an optimum defect width for which R_{SP} is maximum.³⁴ These defects are called *plasmon mirrors*.^{29,34} For increasing defect widths, protuberances and indentations begin to behave differently, except for their negligible contribution to SPP reflection. On the one hand, SPP transmission through protuberances monotonically diminishes at the expense of radiation. The conversion is steeper the higher the defect is. Indentations, however, exhibit an oscillatory pattern with increasing defect width, in such a way that radiation (SPP transmission) increases (decreases), passes through a maximum (minimum), and then tends asymptotically to 0 (1). The oscillation period, the defect width that yields maximum radiation, and the value of this maximum, all depend on the surface height. Note that both protuberances and indentation may behave as *light-emitters*³⁴ (high SPP-light conversion efficiency) for an appropriate (and distinct) range of defect parameters. Below we analyze in detail the behavior of SPP mirrors and light-emitters.

B. Narrow defects: SPP mirrors

Surface defects playing the role of SPP mirrors have been studied experimentally in PSTM configurations.²⁹ This phenomenon has been analyzed for different defect shapes in Ref. 34, where in addition a simple analytical prediction is given through a perturbation-theoretic argument. In the case of Gaussian-shaped defects, the predicted half-width that yields maximum reflection is: $a_{mirr} \approx [2^{1/2} k^R(\omega)]^{-1}$. Our numerical results further corroborate this prediction, since it is seen in Fig. 3 that $a_{mirr}/\lambda \approx 0.1$ no matter what the defect height is [as long as this height does not exceed the range of validity of Eq. (25)]. Nonetheless, the maximum SPP reflection

increases with the defect height, and is slightly larger for indentations.

The electric and magnetic near-field intensities for Gaussian defects, placed at the origin, of width $a/\lambda = 0.1$ and heights $h/\lambda = \pm 0.05$ (protuberance and indentation, respectively) are presented in Figs. 4 and 5, respectively. The near-field maps are quite similar in both cases. The oscillations to the left of the obstacles clearly reveal the interference between the incident and backscattered SPP, their period being $T \approx 2\pi/(2k^R)$, as expected, and their contrast being related to R_{SP} . A bright region is seen to the right of the defects that is due to the strong SPP transmission. Poynting vector maps superimposed on the electric near-field intensity maps confirm the description of the energy flow given above.

The corresponding angular distributions of scattered light (DRC) have been shown in Fig. 2(b). There are no significant qualitative differences between protuberances and indentations, both yielding a fairly structureless angular dependence; quantitatively, an indentation leads to stronger light coupling. The qualitative behavior is somewhat expected: the same perturbation-theoretic argument predicting maximum SPP reflection for a defect width that maximizes the scattering potential [cf. Eq. (8)] at backscattering,³⁴ leads to a mostly uniform SPP coupling into EM waves in the radiative region ($|q| \leq \omega/c$).

C. Wide protuberances: Total light-emitters

The ability of Gaussian-shaped protuberances to couple SPP into light has been pointed out in Ref. 34. Here we analyze in detail the conditions for protuberances and indentations alike to behave as light-emitters with coupling efficiencies beyond 90%, larger than that reported in Ref. 34. Figure 3 above illustrates the discussion.

To begin with, let us focus on protuberances. For widths beyond those producing significant SPP reflection (SPP mirrors), SPP-light conversion increases monotonically whereas, as expected from energy conservation, SPP transmission decays. This variation is faster for higher protuberances. Indeed, the curves in Fig. 3 (bottom) indicate that $\lim_{a \rightarrow \infty} S = 1$ even for the small protuberance. We have found coupling efficiencies beyond 90% in the case of $h/\lambda = 0.2$ and $a/\lambda \geq 3.6$. In Fig. 6, the electric and magnetic near-field intensity maps for one such defect are shown. The absence of oscillations to the left of the defect reveals that SPP reflection is small; SPP transmission is small too (though considerably larger than R_{SP}), as seen on the right-hand side of the defect. A light beam is observed leaving the surface from the defect at near-grazing scattering angles. This energy flow picture is further corroborated by the angular distribution of the DRC shown in Fig. 7, with a maximum at $\theta_s \approx 74^\circ$. Qualitatively, the fact that the metal protuberance enters the vacuum half-space seems

to favor the SPP-photon coupling (playing the role of a *launching platform*).

D. Wide indentations: Light-emitters and SPP total transmission

In the case of wide indentations, however, the behavior of the different outgoing channels differs from that for protuberances, and exhibits a richer phenomenology. Upon increasing the width of the indentation beyond the range of significant SPP reflection (see Fig. 3), SPP transmission reaches a minimum value leading to maximum radiation, and then slowly grows towards *total transmission* (no radiation) in an oscillatory manner. The defect width that yields maximum radiation, its value, and the oscillations depend on the defect height.

To understand such behavior, we plot in Figs. 8 and 9 the electric near-field intensity maps for the higher defects ($h/\lambda = 0.2$) of widths $a/\lambda = 0.3$ and $a/\lambda = 4$, respectively. These widths correspond to the first absolute and sixth subsidiary, maxima in Fig. 3 (bottom), respectively. Both indentations give rise to a negligible amount of SPP reflection (no oscillations to the left of the defect), as expected from Fig. 3 (top). SPP transmission (to the right of the defect) is very small for $a/\lambda = 0.3$, but a strong light beam at grazing scattering is observed ($S = 94\%$). For $a/\lambda = 4$, although most of the energy goes into $T_{SP} = 86.1\%$, a small amount of radiation also at grazing scattering angles is seen [recall that even though for this width a local maximum occurs in S , its value is very small $S = 13.3\%$, see Fig 3 (bottom)]. But what is very illustrative to the discussion on the behavior of the outgoing channels is the near-field within the indentation (strictly speaking, right on top of the indentation region, since we are using an IBC on a flat surface). Oscillations are found therein, the number of minima (one in Fig. 8 and six in Fig. 9) being directly related to the position of the corresponding maxima in the S vs. a curve [see Fig. 3]. Therefore, it can be inferred that the oscillatory behavior of SPP transmission and conversion into light in indentations is governed by a cavity-like effect. In fact, the near field map (not shown here) in the vicinity of any minimum-radiation indentation provides further evidence for this suggestion.

As a consequence, the range of defect widths for which high coupling efficiencies are encountered is far more restrictive for indentations. In fact, in contrast with protuberances, only sufficiently deep indentations ($h/\lambda \geq 0.2$) are capable of producing radiation efficiencies $S > 90\%$, and only for a narrow range of parameters. It seems as if the indentation geometry would somehow hinder grazing light scattering. Therefore, this kind of *light-emitters* might not correlate with any of the reciprocal versions (SPP flashlights) seen in PSTM experiments.^{29,30}

E. Large width limit

Although the energy conservation criterion is reasonably well satisfied in our calculations, even for defects wider than those used in Fig. 3 (we have reached up to $a/\lambda = 20$), one has to be careful when interpreting the results in the limit $a/\lambda \rightarrow \infty$. It turns out that the determination of the behavior of defects in this limit is important, since different tendencies have been encountered for protuberances and indentations (total radiation and transmission, respectively).

The analysis of the appropriate defect width that yields maximum coupling is not simple even if making use of the Born approximation, since it requires the evaluation of the integral of $\hat{s}(q - k^R)$ for all homogeneous waves $|q| < \omega/c$. And yet such an approximation does not properly describe the formally exact numerical calculations. Alternatively, we have carried out an analytic calculation based on the use of a boundary condition similar to the Kirchhoff approximation. The approach relies on the expression for the scattering amplitude in terms of an integral equation along the surface with the magnetic field and its normal derivative inside the integrand (cf. Refs. 37, 38 for the integral equation formulation, and Ref. 3 for its version making use of the IBC on a flat surface). By assuming that the surface magnetic field is given by the incoming SPP, the scattering amplitude reads in the large width limit:

$$\lim_{a/\lambda \rightarrow \infty} R(q, \omega) = 2\pi\delta(q - k^R(\omega))(1 + \pi s_0). \quad (30)$$

Although it does not satisfy energy conservation (not surprisingly, due to the approximation involved), the former result gives an estimation of the limiting behavior shown above (see Fig. 3): SPP transmission saturates for indentations ($s_0 > 0$), whereas protuberances ($s_0 < 0$) tend to decrease SPP transmission (in agreement with the numerical calculations, yet the exact limit is not predicted).

IV. CONCLUSIONS

We have presented a theoretical formulation that describes in a rigorous manner the scattering of a surface plasmon polariton propagating along a planar vacuum-metal interface by a one-dimensional obstacle modeled through an impedance boundary condition. By solving the k -space scattering integral equation upon which the formulation is based, the angular spectrum of the scattered electromagnetic field in the vacuum half-space above the metal surface can be calculated, which in turn allows us to obtain the near electric and magnetic fields, the amplitudes of the reflected and transmitted SPP, and the angular distribution of the intensity of radiated waves resulting from the conversion of SPP into volume waves. A numerical method to solve the scattering integral equation has been put forth.

We have made use of these calculation methods to study the SPP scattering by one-dimensional Gaussian defects, either protuberances or indentations. In particular, the dependence of the scattering process on the surface defect parameters has been analyzed. Several conclusions can be drawn from our results with respect to the behavior of Gaussian protuberances or indentations.

SPP reflection is only significant for very narrow surface defects, with half-widths $a < c/\omega$. Our near field results explicitly show that in this case protuberances and indentations behave alike, the latter reflecting SPP slightly more efficiently. The dependence of the SPP reflection coefficient on the half-width confirms for different defect heights the condition predicted in Ref. 34 of maximum SPP reflection, leading to the *plasmon mirrors* seen in PSTM experiments.²⁹

For wider Gaussian defects, protuberances and indentations yield a entirely different picture, the only common feature being the negligible contribution to SPP reflection. Protuberances, on the one hand, increasingly radiate more light at near grazing scattering angles at the expense of SPP transmission. They behave as *light-emitters* with coupling efficiencies approaching 100% with increasing half-width. The higher the defect is, the larger the SPP-light conversion. On the other hand, indentations tend to total SPP transmission without radiation with increasing half-width. The increase (decrease) of the SPP transmission (light coupling) occurs in an oscillatory manner starting from an absolute minimum (maximum) in transmission (radiation) for small half-widths, the period of the oscillations being related to the defect impedance in a way reminiscent of a cavity-like effect. Interestingly, we have found that for sufficiently deep indentations, this maximum radiation value can be extremely large (even larger than 90%), so that the Gaussian indentation thus behave as a light-emitter.

Our results and discussion provide a thorough picture of the different aspects of SPP scattering by surface defects which, besides being interesting in itself as a scattering process, appears to be useful in a number of related problems.^{14,15,26,27,28,29,30,31,33,34} It is rigorous for one-dimensional defects and indeed sheds light on the two-dimensional case, and can in turn explain and predict experimental results.^{29,30} In this regard, it would be interesting to perform experiments on metal surfaces with defects of controlled profile. With respect to the 2D case, it should be emphasized that the recent work by Shchegrov *et al.*³² for circularly symmetric surface defects reproduces the radiation pattern with peculiar lobes in the azimuthal angle dependence observed experimentally.²⁹ However, further theoretical work is needed that could address more complicated geometries used in the experiments and/or unexplained processes involving surface plasmon-polaritons.^{14,26,31}

ACKNOWLEDGMENTS

This work was supported in part by Army Research Office Grant No. DAAH 0-96-1-0187, and by both the Spanish DGES (Grants No. PB96-0844-C02-02 and PB97-1221) and the Consejo Superior de Investigaciones Científicas. J.A.S.-G. acknowledges fruitful discussions with J. M. Sáiz.

APPENDIX

By discretizing q and p in Eq. (11) and replacing the infinite limits in the integral by sufficiently large finite limits, the following system of linear equations is obtained for the $t_n \equiv T(p_n, \omega)$ unknowns:

$$[K_{mn}]t_n = v_m, \quad (\text{A1})$$

with $v_m \equiv V(q_m|k^R(\omega))$. The matrix elements K_{mn} are given by

$$K_{mn} = \delta_{mn} + M_{mn}, \quad (\text{A2})$$

where δ_{mn} is the Kronecker delta and

$$M_{mn} = -\frac{1}{2\pi}C(\pm k^R(\omega), \omega)V(q_m|\pm k^R(\omega)) \times \left(\pi i + \log \left| \frac{2k^R(\omega) - \Delta q/2}{2k^R(\omega) + \Delta q/2} \right| \right), \quad p_n = \pm k^R(\omega) \quad (\text{A3a})$$

$$= -\frac{1}{2\pi}C(q_m, \omega)V(q_m|p_n) \times \left(\log \left| \frac{p_n + \Delta q/2 - k^R(\omega)}{p_n - \Delta q/2 - k^R(\omega)} \right| + \log \left| \frac{p_n - \Delta q/2 + k^R(\omega)}{p_n + \Delta q/2 + k^R(\omega)} \right| \right), \quad p_n \neq \pm k^R(\omega). \quad (\text{A3b})$$

In obtaining Eqs. (A3), the explicit form of $G_0(q, \omega)$ shown in Eq. (15) has been taken into account in calculating the corresponding integrals over the sampling intervals $[p_n - \Delta q/2, p_n + \Delta q/2]$.

¹ *Surface Polaritons*, edited by V. M. Agranovich and D. L. Mills (North-Holland, Amsterdam, 1982); *Surface Polaritons on Smooth and Rough Surfaces and on Gratings*, edited by H. Raether (Springer, Berlin, 1988).

² F. Pincemin, A. A. Maradudin, A. D. Boardman, and J. J. Greffet, Phys. Rev. B **50**, 15 261 (1994).

³ J. A. Sánchez-Gil, Phys. Rev. B **53**, 10 317 (1996).

- ⁴ S. C. Kitson, W. L. Barnes, and J. R. Sambles, Phys. Rev. Lett. **77**, 2670 (1996).
- ⁵ F. Pincemin and J. J. Greffet, J. Opt. Soc. Am. B **13**, 1499 (1996).
- ⁶ J. A. Sánchez-Gil and A. A. Maradudin, Phys. Rev. B **56**, 1103 (1997).
- ⁷ F. Pincemin, A. Sentenac, and J. J. Greffet, J. Opt. Soc. Am. A **11**, 1117 (1994).
- ⁸ P. J. Valle, F. Moreno, J. M. Sáiz, and F. González, Phys. Rev. B **51**, 13 681 (1995).
- ⁹ A. Madrazo and M. Nieto-Vesperinas, J. Opt. Soc. Am. A **12**, 1298 (1995); J. Opt. Soc. Am. A **13**, 785 (1996); Appl. Phys. Lett. **70**, 31 (1997).
- ¹⁰ F. Pincemin, A. Sentenac, and J. J. Greffet, Opt. Commun. **114**, 13 (1995).
- ¹¹ C. S. West and K. A. O'Donnell, J. Opt. Soc. Am. A **12**, 390 (1995); Opt. Lett. **21**, 1 (1996).
- ¹² A. A. Maradudin, A. R. McGurn, and E. R. Méndez, J. Opt. Soc. Am. A **12**, 2500 (1995).
- ¹³ K. A. O'Donnell, C. S. West, and E. R. Méndez, Phys. Rev. B **57**, 13 209(1998).
- ¹⁴ T. W. Ebbesen, H. J. Lezec, H. F. Ghaemi, T. Thio, and P. A. Wolff, Nature **391**, 667 (1998); H. F. Ghaemi, T. Thio, D. E. Grupp, T. W. Ebbesen, and H. J. Lezec, Phys. Rev. B **58**, 6779 (1998).
- ¹⁵ U. Schröter and D. Heitmann, Phys. Rev. B **58**, 15 419 (1998).
- ¹⁶ V. M. Shalaev, Phys. Rep. **272**, 61 (1996).
- ¹⁷ F. J. Vidal and J. B. Pendry, Phys. Rev. Lett. **77**, 1163 (1996).
- ¹⁸ J. A. Sánchez-Gil and J. V. García-Ramos, Opt. Commun. **134**, 11 (1997); J. Chem. Phys. **108**, 317 (1998).
- ¹⁹ C. Nylander, B. Liedberg, and T. Lindt, Sensors Actuators **3**, 79 (1982).
- ²⁰ *Near Field Optics*, edited by D. W. Pohl and D. Courjon (Kluwer, The Netherlands, 1993).
- ²¹ R. C. Reddick, R. J. Warmack, and T. L. Ferrell, Phys. Rev. B **39**, 767 (1989).
- ²² O. Marti, H. Bielefeldt, B. Hecht, S. Herminghaus, P. Leiderer, and J. Mlynek, Opt. Commun. **96**, 225 (1993).
- ²³ P. M. Adam, L. Salomon, F. de Fornel, and J. P. Goudonnet, Phys. Rev. B **48**, 2680 (1993); P. Dawson, F. de Fornel, and J. P. Goudonnet, Phys. Rev. Lett. **72**, 2927 (1994).
- ²⁴ S. Bozhevolnyi, B. Vohnsen, I. I. Smolyaninov, and A. V. Zyats, Opt. Commun. **117**, 417 (1995); S. Bozhevolnyi, I. I. Smolyaninov, and A. V. Zyats, Phys. Rev. B **51**, 17 916 (1995).
- ²⁵ D. P. Tsai, J. Kovacs, Z. Wang, M. Moskovits, V. M. Shalaev, J. S. Suh, and R. Botet, Phys. Rev. Lett. **72**, 4149 (1994).
- ²⁶ S. Nie and S. R. Emory, Science **275**, 1102 (1997).
- ²⁷ T. Klar, M. Perner, S. Grosse, G. von Plessen, W. Spirkl, and J. Feldmann, Phys. Rev. Lett. **80**, 4249 (1998).
- ²⁸ I. I. Smolyaninov, D. L. Mazzoni, and C. C. Davis, Appl. Phys. Lett. **67**, 3859 (1995).
- ²⁹ I. I. Smolyaninov, D. L. Mazzoni, and C. C. Davis, Phys. Rev. Lett. **77**, 3877 (1996); I. I. Smolyaninov, D. L. Mazzoni, J. Mait, and C. C. Davis, Phys. Rev. B **56**, 1601 (1997).
- ³⁰ S. Bozhevolnyi, Phys. Rev. B **54**, 8177 (1996); S. Bozhevol-

- nyi and F. A. Pudonin, Phys. Rev. Lett. **78**, 2823 (1997).
- ³¹ I. I. Smolyaninov, W. Atia, and C. C. Davis, Phys. Rev. B **59**, 2454 (1999).
- ³² A. V. Shchegrov, I. V. Novikov, and A. A. Maradudin, Phys. Rev. Lett. **78**, 4269 (1997).
- ³³ M. Pascual, W. Zierau, T. A. Leskova, and A. A. Maradudin, Opt. Commun. **155**, 351 (1998).
- ³⁴ J. A. Sánchez-Gil, Appl. Phys. Lett. **73**, 3509 (1998).
- ³⁵ A. A. Maradudin, in *Topics in Condensed Matter Physics*, edited by M. P. Das (Nova, New York, 1994).
- ³⁶ In so doing, we are assuming that $T(q, \omega)$ as a function of complex q is analytical and behaves appropriately in the limit $|q| \rightarrow \infty$.
- ³⁷ J. A. Sánchez-Gil and M. Nieto-Vesperinas, J. Opt. Soc. Am. A **8**, 1270 (1991).
- ³⁸ A. A. Maradudin, T. R. Michel, A. R. McGurn, and E. R. Méndez, Ann Phys. (NY) **203**, 255 (1990).

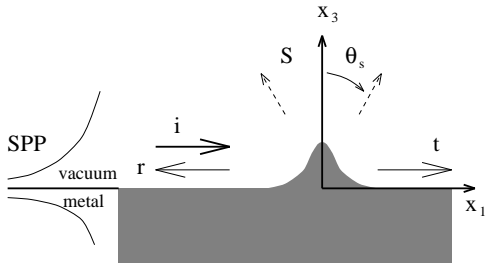


FIG. 1. Illustration of the scattering geometry.

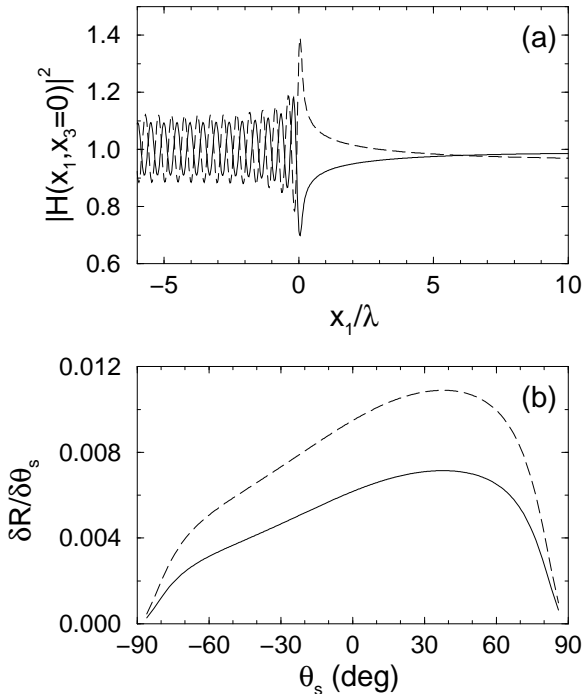


FIG. 2. (a) Square modulus of the total surface magnetic field and (b) DRC resulting from the scattering of a SPP of frequency $\hbar\omega = 1.96$ eV ($\lambda = 632.8$ nm) by Gaussian defects on a silver surface ($\epsilon = -17.2$) of half-width $a = 0.1\lambda$. Solid curve: $h = 0.05\lambda$ (protuberance); dashed curve: $h = -0.05\lambda$ (indentation).

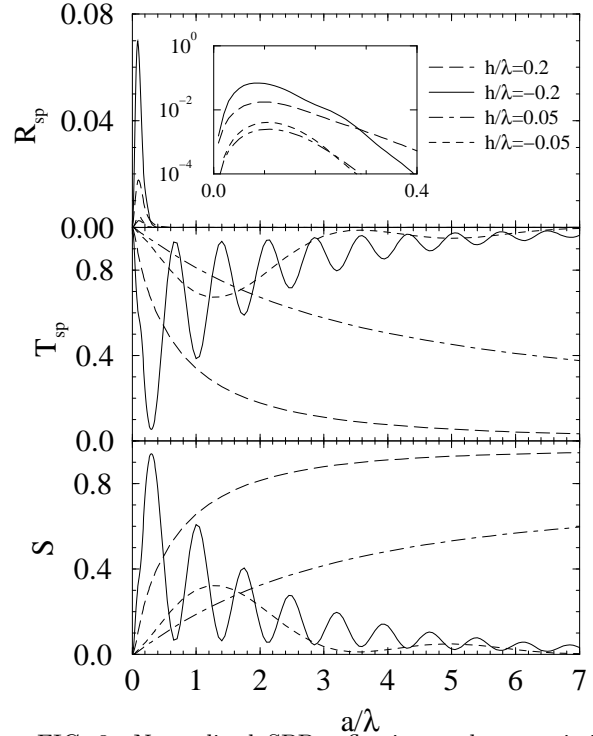


FIG. 3. Normalized SPP reflection and transmission coefficients (R_{SP} and T_{SP} , respectively), and total radiated energy S , as functions of the Gaussian defect half-width: $\hbar\omega = 1.96$ eV ($\lambda = 632.8$ nm) and $\epsilon = -17.2$. Long-dashed curve: $h = 0.2\lambda$; solid curve: $h = -0.2\lambda$; dot-dashed curve: $h = 0.05\lambda$; dashed curve: $h = -0.05\lambda$. The inset zooms in the reflection coefficient in a semi-log scale for narrow defects.

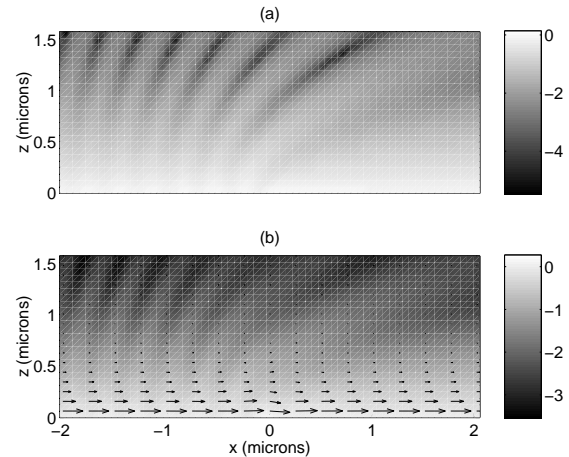


FIG. 4. Near field intensity distribution (in a log scale) resulting from the scattering of a SPP of frequency $\hbar\omega = 1.96$ eV ($\lambda = 632.8$ nm) by a Gaussian protuberance on a silver surface ($\epsilon = -17.2$) of half-width $a = 0.1\lambda$ and height $h = 0.05\lambda$. (a) Magnetic field intensity and (b) Electric field intensity and Poynting vector.

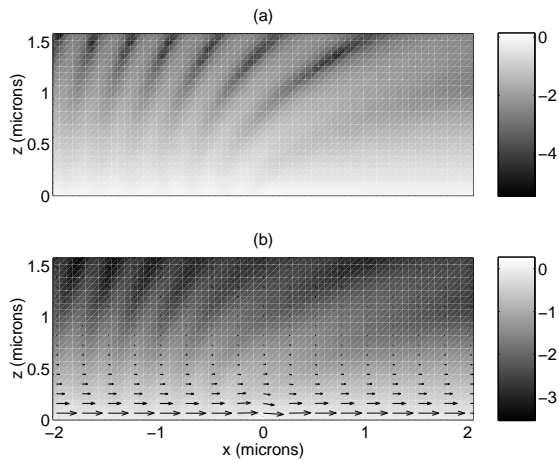


FIG. 5. Same as in Fig. 4 but for a Gaussian indentation $h = -0.05\lambda$.

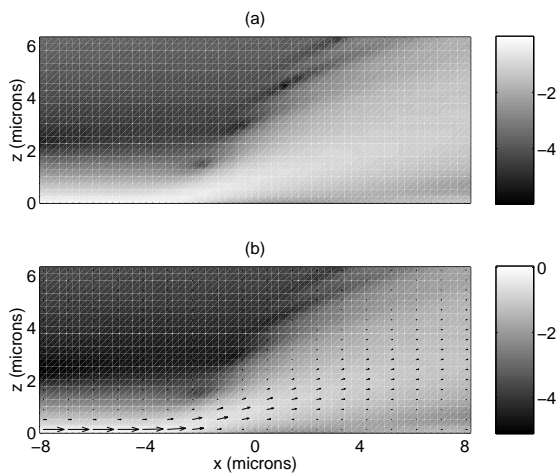


FIG. 6. Same as in Fig. 4 but for $h = 2\lambda$ and $a = 4\lambda$ (and for a larger near field area).

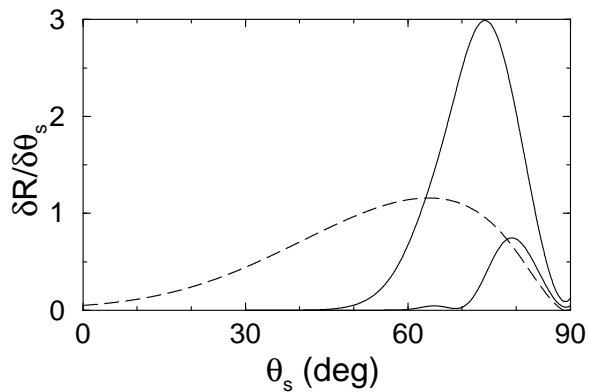


FIG. 7. DRC as in Fig. 2(b) but for: Upper solid curve, $h = 2\lambda$ and $a = 4\lambda$; dashed curve, $h = -2\lambda$ and $a = 0.3\lambda$; lower solid curve, $h = -2\lambda$ and $a = 4\lambda$.

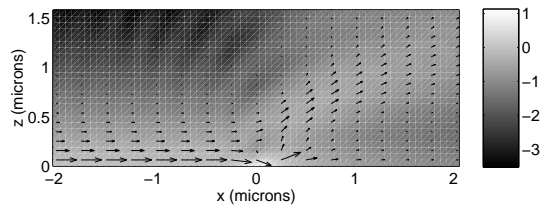


FIG. 8. Same as in Fig. 4(b) but for $h = -2\lambda$ and $a = 0.3\lambda$.

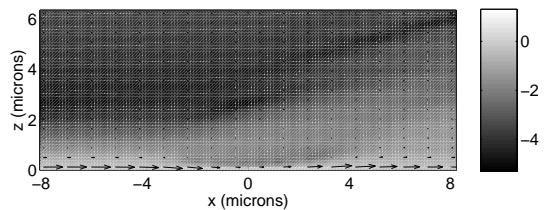


FIG. 9. Same as in Fig. 6(b) but for $h = -2\lambda$ and $a = 4\lambda$.